Scaling snow observations from the point to the grid element: Implications for observation network design

Noah P. Molotch

Cooperative Institute for Research in Environmental Sciences, University of Colorado, Boulder, Colorado, USA

Roger C. Bales

Division of Engineering, University of California, Merced, California, USA

Received 2 May 2005; revised 2 August 2005; accepted 16 August 2005; published 17 November 2005.

[1] The spatial distribution of snow water equivalent (SWE) within 16-, 4-, and 1-km^2 grid elements surrounding six snow telemetry (SNOTEL) stations in the Rio Grande headwaters was characterized using field observations of snowpack properties, satellite data, binary regression tree models, and a spatially distributed net radiation/temperature index snowpack mass balance model. In some cases, SNOTEL SWE values were 200% greater than mean grid element SWE. Analyses designed to identify the optimal location for measuring mean grid element SWE accumulation indicated that only 2.4% of each grid element satisfied the criteria of optimality. Similar analyses for the ablation season showed that point SWE and mean grid element SWE were highly correlated ($r = 0.73$) in areas with relatively persistent snow cover. These locations did not overlap in space with areas deemed optimal at maximum accumulation; areas with persistent snow cover have relatively high accumulation rates. Therefore future observations may need to be placed with the specific objective of representing either accumulation or ablation season processes. These results have implications for large-scale studies that require ground observations for updating purposes; we show an example of this utility using the SWE product of the National Operational Hydrologic Remote Sensing Center. Furthermore, the relatively consistent spatial patterns of snow accumulation and melt have implications for future observation network design in that results from short-term studies (e.g., 2 years) can be used to design long-term observation networks.

Citation: Molotch, N. P., and R. C. Bales (2005), Scaling snow observations from the point to the grid element: Implications for observation network design, *Water Resour. Res.*, *41*, W11421, doi:10.1029/2005WR004229.

1. Introduction

[2] In seasonally snow covered mountainous regions, the spatial resolution of distributed hydrologic models is largely dictated by the scale of the available input data [*Blöschl*, 1999]. The spatial distribution of snow water equivalent (SWE) is a particularly important state variable in many of these simulations as it provides the majority of the water input to the system and dramatically influences energy exchange between the land surface and the atmosphere. The ideal spatial resolution for estimating SWE distribution reduces subgrid element heterogeneity to a level where the majority of the variability in the system can be modeled explicitly [*Blöschl*, 1999]. However, a certain amount of variability has to be ignored or parameterized [*Beven*, 1995].

[3] Managed by the Natural Resource Conservation Service (NRCS), the snow telemetry (SNOTEL) network provides daily snow water equivalent measurements at 768 stations across the western United States. SNOTEL stations, which generally consist of a snow pillow, air temperature sensor, and a storage precipitation gauge, replace the manual snow courses that provide information for empirical water supply forecasts. Since the data are used in regression-based water supply forecast models, snow courses were placed in areas that are representative of the water producing regions of a watershed [*U.S. Soil Conservation Service*, 1972]. Because the main criteria for snow course site selection were accessibility and protection from public disturbance (M. Gillespie, NRCS, personal communication, 2004), snow courses and SNOTEL stations may not provide the quantitative, spatial snowpack information needed for spatially distributed modeling. Nevertheless, the network has been used to estimate the spatial distribution of SWE [*Fassnacht et al.*, 2003; *Molotch et al.*, 2004b] and to update snowpack model state variables within hydrologic models [*Carroll et al.*, 2001]. The use of SNOTEL data in these applications assumes that observed SWE at a given SNOTEL station is representative of the corresponding grid element. Thus there is a need to evaluate the validity of this assumption by defining the continuum of SWE within grid elements encompassing SNOTEL stations.

[4] Future spatial modeling and measurement of hydrometeorological processes in mountainous regions will require improved observational capabilities [*Consortium of Universities for the Advancement of Hydrologic Science Inc.*, 2003; *GEWEX America's Prediction Project*, 2003]. Hence a statistically unbiased approach for selecting the

0043-1397/05/2005WR004229$09.00

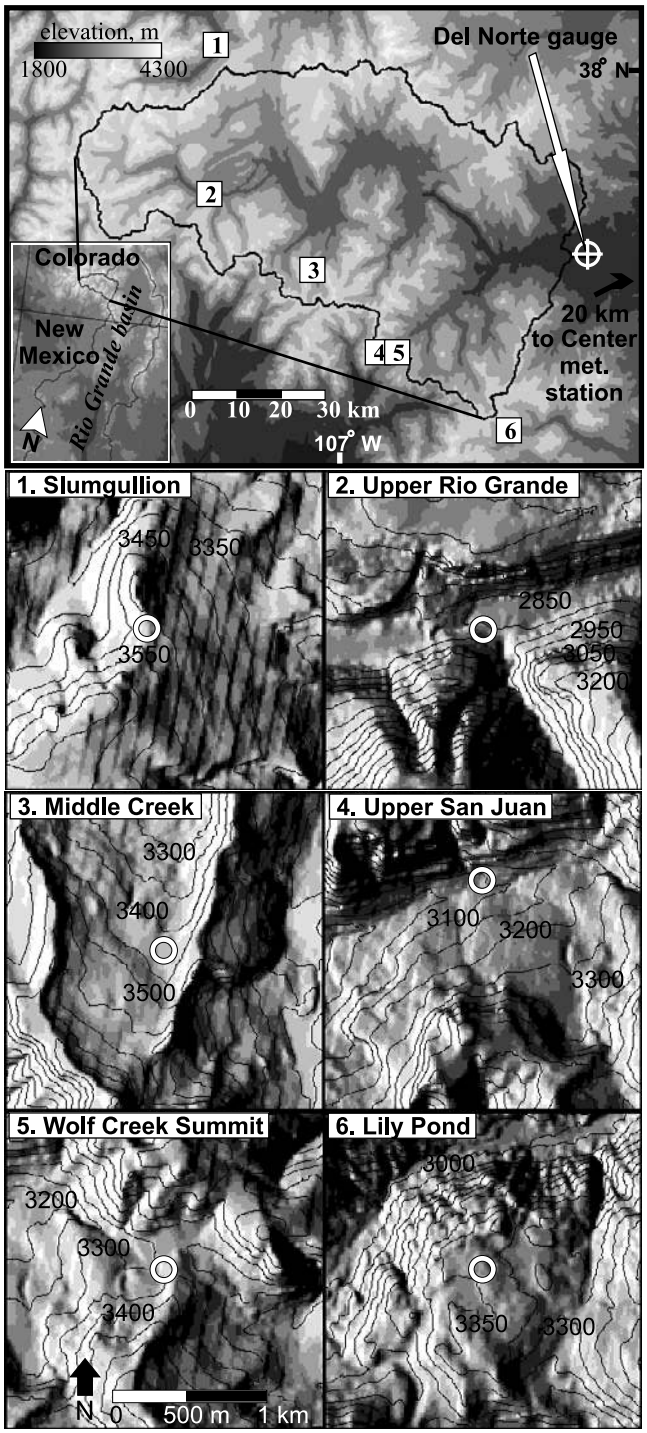

Figure 1. The Rio Grande above Del Norte and the Slumgullion (1), Upper Rio Grande (2), Middle Creek (3), Upper San Juan (4), Wolf Creek Summit (5), and Lily Pond (6) SNOTEL sites. White rings indicate the locations of the SNOTEL sites. Location of the Colorado State University San Luis Valley Research Center at Center Colorado is also indicated.

most representative locations for future snowpack observations is needed.

[5] Midlatitude alpine and subalpine regions often exhibit a distinct snow accumulation season in which snowmelt between snowfall events is relatively insignificant with respect to the snowpack mass balance. Conversely, a distinct ablation season often exists in which inputs of precipitation during the melt season are relatively insignificant to the snowpack mass balance. Thus physically based techniques for upscaling ground-based snow water equivalent observations should represent both snow accumulation and snow ablation processes.

[6] Small-scale snow distribution studies have shown that the relationships between snow accumulation and physiographic variables are nonlinear [*Elder et al.*, 1998; *Molotch et al.*, 2005]. Regression tree snow depth models have been used to explore these nonlinear relationships with considerable success [*Balk and Elder*, 2000; *Elder et al.*, 1998; *Erxleben et al.*, 2002; *Molotch et al.*, 2005; *Winstral et al.*, 2002] and therefore can be used to determine how independent variables control the continuum of snow distribution over a given area.

[7] During the snow ablation season, the mass balance of the snowpack can be determined by knowing two of the following three variables: (1) SWE accumulation at the beginning of melt, (2) the melt rate, and (3) the depletion rate of snow covered area (SCA) [*Liston*, 1999]. In midlatitude mountainous regions, where radiative fluxes dominate snowmelt [*Cline*, 1997], snowmelt rates can be adequately simulated using a temperature index model that explicitly includes net radiation [*Brubaker et al.*, 1996; *Molotch et al.*, 2004a]. Modeled snowmelt can be integrated over the time required to melt all of the snow in a given area; the initial SWE over that area is equal to the integrated value [*Cline et al.*, 1998; *Molotch et al.*, 2004a].

[8] We use the aforementioned snow accumulation and ablation models to characterize the spatial variability of SWE surrounding six SNOTEL stations in and around the Rio Grande headwaters (Figure 1). More specifically, we use binary regression tree models, physiographic variables, and detailed observations of snow depth and snow density to assess SNOTEL representativeness at maximum accumulation; and by proxy the accumulation season. A temperature index mass balance model which explicitly includes net radiation was then used to reconstruct daily SWE distribution [*Molotch et al.*, 2004a] and temporal trends in SNOTEL representativeness. As part of this assessment we present an approach for determining the most representative area for future observations.

[9] Three questions are addressed. First, what is the distribution of SWE within grid elements of various resolutions (i.e., 16, 4, and 1 km^2) encompassing the SNOTEL sites and how representative are these sites relative to the mean of the distribution? Second, what are the temporal trends in SNOTEL representativeness throughout the snowmelt season? Finally, what is the optimal location for future observations of SWE for the purpose of upscaling to the grid element?

2. Study Area

[10] This study was conducted in an area surrounding the Rio Grande headwaters in the San Juan Mountains of southern Colorado (Figure 1). Nested study areas surrounding six SNOTEL sites were included in this research. Additional meteorological data used in this research (i.e., relative humidity, air temperature, and wind speed and direction) were obtained from the Colorado State University

Table 1. Attributes of the Six SNOTEL Sites in the Rio Grande Headwaters Used in the Analysis

Site[a]	Forest Density,[b] %	Elevation,[c] m	Installed[c]	Maximum SWE,[c,d] cm
1	82	3581	1980	42
2	62	2855	1987	17
3	40	3430	1980	53
4	71	3089	1979	83
5	76	3331	1987	94
6	68	3374	1980	43

[a]Sites 1–6 are numbered as in Figure 1.
[b]Source: USGS EROS data center.
[c]Source: NRCS National Water and Climate Center.
[d]Values are average annual maximum Snow Water Equivalent (SWE) from installation year to 2002.

San Luis Valley Research Center at Center, Colorado (hereafter referred to as the Center meteorological station) (106°8′38″W, 37°42′24″N) (Figure 1). Physiographic attributes of the sites and average annual maximum SWE accumulations are shown in Table 1.

3. Study Period

[11] This study was conducted from maximum SWE accumulation (Table 2) through the end of the 2001 and 2002 snowmelt seasons. Maximum SWE accumulation at the six SNOTEL sites averaged 128% and 34% of historical means for water years 2001 and 2002, respectively. The accumulation season is described below solely for background on snowpack condition at maximum accumulation. In 2001 the snow accumulation season began early with above average precipitation during the months of October and November. A drier than average December and early January was followed by above average precipitation from late January until the end of April.

[12] In 2002 below average precipitation was recorded at the six sites throughout the water year. The period from 1 December to 1 March was particularly dry with total precipitation less than 10 cm on average. This cold dry period caused substantial vapor gradients within the snowpack; faceted snow layers persisted from the ground surface to the snow/atmosphere interface in many locations. The snow accumulation season terminated relatively early, with little precipitation recorded after 20 March. The snowmelt season commenced and concluded approximately one month earlier in 2002 versus 2001 (Table 2). Precipitation during the snowmelt season was greater in 2001.

4. Methods

[13] Two approaches to estimating the spatial distribution of SWE within the grid elements were applied. The first approach used intensive field surveys of snow depth and density, binary regression tree models, and remotely sensed SCA data to estimate SWE near the time of maximum accumulation. The second approach used remotely sensed SCA data and a net radiation/temperature index mass balance model [*Molotch et al.*, 2004a] to reconstruct daily SWE distributions throughout the snowmelt season. The second approach was evaluated by comparing the pixel-specific reconstructed SWE estimates, at the time of the field surveys, with regression tree SWE estimates as they are based on field observations. Above and hereafter the term grid element is used to signify the 16-, 4-, and 1-km^2 areas surrounding the SNOTEL sites. The term pixel is used to signify the 30-m scale at which we model subgrid element SWE distributions.

4.1. Field Methods

[14] Snow depth and density data were collected around the six SNOTEL sites on 22–27 April 2001 and 3–12 April 2002. At all six sites, snow depth and density measurements were made along four, 500-m-long transects extending linearly in cardinal directions from the snow pillow (Figure 2). Triplicate snow density measurements were made at 100-m intervals along these transects using a Federal Sampler and locations were recorded using a global positioning system (GPS). Snow depth measurements were made using a composite graphite probe at 25-m intervals along these transects. Federal Sampler snow density observations were multiplied by 0.9 to account for sampling errors [*Gray and Male*, 1981]. Snow pits were excavated within five meters of the snow pillow and snow density was measured at 10-cm vertical intervals using a 1000 cc stainless steel snow cutter. Three to five Federal Sampler measurements were made adjacent to the snow pit (Figure 2). Snow depth measurements were also made at 1-m intervals along 15-m transects extending from the snow pillows in cardinal directions (Figure 2). The snow depth on a given snow pillow was estimated using the average value of the four closest snow depth measurements, the depth of the snow pit, and the ratio of the SWE measured on the pillow and the snow density measured in the snow pit.

[15] At the Slumgullion and Upper San Juan sites additional snow depth measurements were made at approximately 250-m intervals in an evenly spaced grid pattern, covering a total area of approximately 4 km^2 (Figure 2). At each point, three depth measurements were collected 5 m apart from one another with the center location recorded using a GPS. Site locations were initially determined using GPS to determine distance from the SNOTEL site. Unlike the measurements made along the 500-m transects, these measurements were repeated on 27 May to 2 June 2001 and on 5–9 May 2002. Measurements were shifted to the south of the Upper San Juan study area by approximately 1 km because of the inaccessibility of the steep terrain to the north of the site.

Table 2. Dates of Annual Maximum Snow Water Equivalent and Snow Disappearance (SWE = 0) at the Six SNOTEL Sites, 2001 and 2002[a]

	Date of Maximum SWE		Date of SWE = 0		Melt Season Precipitation, cm	
Site[b]	2001	2002	2001	2002	2001	2002
1	24 Apr	17 Apr	1 Jun	13 May	5.33	0.76
2	15 Apr	12 Mar	11 May	25 Mar	3.05	1.02
3	23 Apr	22 Mar	9 Jun	22 Apr	3.56	3.05
4	23 Apr	27 Mar	2 Jun	26 Apr	4.32	2.54
5	28 Apr	18 Apr	21 Jun	25 May	3.56	0.00
6	23 Apr	21 Mar	20 May	22 Apr	3.56	2.03

[a]Snowmelt season precipitation is also shown.
[b]Sites 1–6 are numbered as in Figure 1.

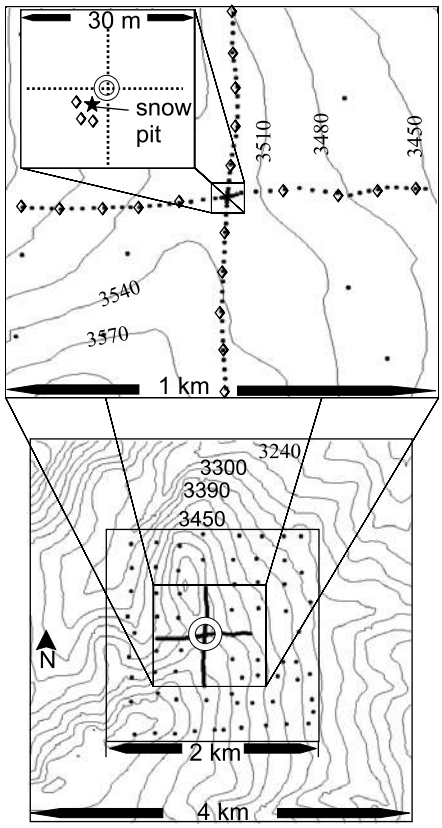

Figure 2. Location of snow density and snow depth measurements (dots) around the Slumgullion SNOTEL site (white ring). Federal sampler measurements are indicated by diamonds in the 1-km^2 inset. This nested design was duplicated at the Upper San Juan SNOTEL site. The sampling design in the 1-km^2 inset was duplicated at the Upper Rio Grande, Middle Creek, Wolf Creek Summit, and Lily Pond sites.

[16] The April 2001 sampling protocol at the Middle Creek site differed from that described above because we were unable to locate the SNOTEL site until late in the day. Snow depth measurements were made along north/south transects to the east of the SNOTEL site until the site was found.

[17] On average, the number of snow depth and density measurements made at each of the six sites in 2001 was 184 and 15, respectively. In 2002, the average number of snow depth and density measurements made was 159 and 16, respectively.

4.2. Physiographic Variables

[18] Using a geographical information system (GIS), the topographic variables elevation, slope and aspect were obtained from the level 1 standard 7.5-min, 30-m resolution, U.S. Geological Survey digital elevation model (DEM).

[19] The TOPQUAD algorithm [*Dozier*, 1980] was used to calculate a solar radiation index assuming clear-sky conditions. Daily integrated net solar radiation was calculated for each 30-m pixel within the study area on the 15th of each month for the period November–May, 2001 and 2002. The solar radiation index was calculated as the sum of daily integrated surfaces from 15 November to the 15th of the respective month of the snow survey.

[20] The mean maximum upwind slope, *Sx*, is a temporally invariant terrain-based parameter designed to capture the variability in snow deposition as a result of wind redistribution [*Molotch et al.*, 2005; *Winstral et al.*, 2002]. The DEM and relative humidity, wind speed, and wind direction data from the Center meteorological station were used to calculate the maximum upwind slope [*Molotch et al.*, 2005; *Winstral et al.*, 2002].

[21] Vegetation density can control snow distribution by altering the energy balance at the snow/atmosphere interface, intercepting snowfall and by influencing the surface roughness and the wind fields that transport snow [*Gray and Male*, 1981]. As a proxy for vegetation density we use forest covered area which we determined from Landsat enhanced thematic mapper (ETM+) derived fractional SCA:

$$F_c = 100 - \mathrm{SCA_s} \tag{1}$$

Where F_c is the forest covered area (percent) and $\mathrm{SCA_s}$ is the fractional SCA (percent) on 1 April, 2001. Methods used to derive fractional SCA are described later in this section. Fractional SCA can provide sufficient estimates of forest covered area provided there is continuous snow cover on the ground and there is no snow in the tree canopy (R. E. Davis, personal communication, 2005); such conditions were present on 1 April 2001. More complex approaches for deriving forest covered area are beyond the scope of this work.

[22] The selection of the variables described above was based on results of previous studies [*Balk and Elder*, 2000; *Elder et al.*, 1998; *Erxleben et al.*, 2002; *Molotch et al.*, 2005; *Winstral et al.*, 2002] that have illustrated the ability of these variables to explain snow distribution.

4.3. Binary Regression Trees

[23] We interpolated point snow depth observations (i.e., the dependent variable) using binary regression tree models. Various combinations of the aforementioned independent variables were used to predict snow depth in a nonlinear hierarchical fashion [*Molotch et al.*, 2005]. Snow depth data were binned into increasingly homogeneous subsets using binary recursive partitioning [*Chambers and Hastie*, 1993]. The techniques used to construct regression trees and perform cross validation are described in detail by *Molotch et al.* [2005].

[24] The ability of inverse Distance Weighting (IDW), kriging and cokriging (with the same 30-m resolution independent variables) to distribute snow depth residuals from the regression tree models was assessed following the methods of *Molotch et al.* [2005]. Spherical, Gaussian and exponential models were fit to the variograms and compared. The models resulting in the lowest root-mean-square errors (RMSE) were selected. Anisotropic variance structure was assessed and determined nonexistent.

[25] The observed snow depths at the SNOTEL sites were compared to the statistical distribution of the final modeled snow depth over the surrounding 16, 4, and 1-km^2 grid elements to assess SNOTEL representativeness.

[26] Snow density observations were interpolated using multivariate regression models that included all aforementioned independent variables [*Erxleben et al.*, 2002; *Molotch et al.*, 2005].

[27] The spatially distributed snow depth estimates were also used to identify the optimal location for future observations. The mean modeled snow depth of each simulation was subtracted from the snow depth estimate of each pixel to create spatially distributed estimates of deviance from the mean value. The absolute values of the April 2001 and 2002 deviation surfaces were summed to derive spatially distributed estimates of cumulative, absolute deviance from the mean. Areas with the lowest deviance from the mean were identified as the optimal locations for future observations. The range of the physiographic conditions of these areas was determined and compared to the conditions at the current SNOTEL sites. SWE was not used for defining the optimal site location because there is more uncertainty in distributed SWE estimates than in distributed snow depth estimates; regression tree models predict snow depth whereas SWE also includes distributed estimates of snow density. Furthermore, exploring the structure of the regression tree snow depth models reveals the physiographic conditions required for representative measurements.

[28] For each regression tree simulation the maximum SWE (m) of each pixel, p, within each study area was determined:

$$\mathrm{SWE}_p = d_p(\rho_s/\rho_w)\mathrm{SCA}_p \tag{2}$$

Where d_p (m) is the modeled snow depth, ρ_s (kg m^{-3}) is the modeled snow density, ρ_w is the density of water (1000 kg m^{-3}), and SCA_p is the fractional snow covered area (described below).

[29] The measured SWE at the SNOTEL sites were graphically compared to the spatial statistical distribution of the regression-tree-modeled SWE of the surrounding 16-, 4-, and 1-km^2 grid elements to assess SNOTEL representativeness.

4.4. Snow-Covered Area

[30] Satellite imagery from ETM+ on 17 April 2001 and 4 April 2002 were used to construct fractional SCA images across the study areas using the direct spectral unmixing algorithm of *Painter et al.* [2003]. Cloud masks were derived manually based on the radiances observed in ETM+ bands 3 and 4. ETM+ data acquired on 1 April, 4 June, 20 June, and 7 July 2001, and 16 March, 6 May, and 22 May 2002 were also processed for fractional SCA for use in snowmelt modeling.

4.5. Snow Water Equivalent Reconstruction

[31] In the absence of significant precipitation inputs, the ablation season mass balance of the snowpack can be approximated as

$$\mathrm{SWE}_n = \mathrm{SWE}_0 - \sum_{j=1}^{n} M_j \tag{3}$$

where M_j is the melt flux at time step j, SWE_n is the SWE of the pixel at time step n, and SWE_0 is the initial SWE. Daily SWE estimates were obtained by manipulating (3) in a manner similar to *Cline et al.* [1998]; when

$$\mathrm{SWE}_n = 0,\ \mathrm{SWE}_0 = \sum_{j=1}^{n} M_j \tag{4}$$

[32] Here SWE_0 is treated as each daily time step from 1 March to 31 July. This time period was chosen as it encompasses the 2001 and 2002 snowmelt seasons (i.e., from maximum SWE to SWE = 0) for any given pixel in the modeling domain. This approach allows us to simulate daily SWE distributions as opposed to the single initial time step simulated by *Cline et al.* [1998]. The time step at which SWE_n equals zero was determined from remotely sensed SCA data; when SCA_n is equal to 0, SWE_n is equal to 0. Pixel-specific melt flux was estimated as [*Brubaker et al.*, 1996]

$$M_j = \left(T_d * a_r + R_n * M_q\right) * \mathrm{SCA}_j \tag{5}$$

Where T_d is the number of degree days (i.e., the average daily air temperature above 0°C), a_r is the degree day coefficient (cm °C^{-1} d^{-1}), R_n is the average daily net radiation above 0 W m^{-2}, and M_q is a simple energy to water depth conversion (0.026 cm W^{-1} m^2 d^{-1}). Vertical melt flux (parenthetic terms in (5)) was scaled by estimates of fractional SCA (values range from 0 to 1) using pixel-specific snow cover depletion curves:

$$\mathrm{SCA}_j = \mathrm{SCA}_i - \left[(\mathrm{SCA}_i - \mathrm{SCA}_k)\Big/\left(\sum_{i=1}^{n} M_i - \sum_{k=1}^{n} M_k\right)\right] * \left[\sum_{i=1}^{n} M_i - \sum_{j=1}^{n} M_j\right] \tag{6}$$

Where SCA_j is the estimated fractional SCA at time step j, SCA_i and SCA_k are Landsat ETM+-observed fractional SCA values preceding and subsequent to time step j, respectively, and $\sum_{i=1}^{n} M_i$ and $\sum_{k=1}^{n} M_k$ are the vertical melt flux summation values corresponding to Landsat ETM+ acquisition time steps i and k, respectively.

[33] This net radiation/temperature index approach was used instead of a physically based model for three reasons. First, wind speed observations, required for physically based models, are not made at SNOTEL stations; extrapolating wind observations from distant locations (e.g., >50 km) over complex terrain would introduce significant uncertainty. Second, we want to maintain transferability of our approach by using a relatively simple technique; here we study only 6 of 768 SNOTEL stations in the western United States. Third, this approach has proven to adequately reconstruct SWE distribution in mountainous environments [*Molotch et al.*, 2004a] as it explicitly represents radiative fluxes which account for the majority of total energy exchange at the snowpack/atmosphere interface [*Cline*, 1997; *Marks and Dozier*, 1992].

[34] Daily SWE empirical cumulative distribution plots were generated for the six study sites and compared with SNOTEL SWE values. For each daily time step SNOTEL SWE, $\mathrm{SWE}_{s,j}$ values were divided by the mean modeled SWE, $\mathrm{SWE}_{a,j}$ within the 16-, 4-, and 1-km^2 grid elements in order to derive a scaling coefficient, $C_{s,j}$ relating SNOTEL SWE to the SWE of the grid element:

$$C_{s,j} = \frac{\mathrm{SWE}_{s,j}}{\mathrm{SWE}_{a,j}} \tag{7}$$

Given the inherent spatial variability in snowmelt rates, the scaling coefficients are likely to change throughout the snowmelt season. Thus a linear least squares fit between SNOTEL scaling coefficients and accumulated degree days was developed to predict the scaling coefficients. Accumulated degree days were determined by summing (throughout the snowmelt season) the observed average daily air temperatures above 0°C. Accumulated degree days were used as the explanatory variable because air temperature is measured at SNOTEL sites whereas other important variables that control snowmelt, such as solar radiation are not. Hence transferability of our approach to other SNOTEL sites is ensured.

[35] To identify the optimal location for future observations scaling coefficients were calculated for each 30-m pixel within the 16-, 4-, and 1-km^2 grid elements:

$$C_{p,j} = \frac{\mathrm{SWE}_{p,j}}{\mathrm{SWE}_{a,j}} \tag{8}$$

where all variables are the same as in (7) only the term for SNOTEL SWE is replaced with pixel-specific SWE indicated by the subscript p. A linear least squares fit was then developed between pixel-specific scaling coefficients and pixel-specific estimates of accumulated degree-days derived from the spatial estimates of air temperature described below. Spatially distributed estimates of correlations were then mapped for 2001 and 2002 independently. Areas in which correlations were consistently highest were determined optimal locations for future observations of ablation season SWE.

[36] The degree-day value, T_d, was spatially distributed using an environmental lapse rate and a 30-m DEM [*Daly et al.*, 1994; *Thornton et al.*, 1997; *Willmott and Matsuura*, 1995]. Lapse rates were determined on a daily basis from air temperature observations at the SNOTEL station within the modeling domain and the next nearest meteorological station (i.e., SNOTEL station or the Center meteorological station). The degree-day coefficient, a_r, was calculated using the standard bulk transfer parameterization [*Brubaker et al.*, 1996] and average observed values of wind speed, relative humidity and air temperature observed at the Center meteorological station over the modeling period. Surface roughness (0.0005 m) and other assumptions were consistent with those of *Brubaker et al.* [1996]. Stability corrections were calculated using the methods of *Kustas et al.* [1994] with specific humidity calculated from observations of air temperature and relative humidity.

[37] Net radiation, R_n, was calculated as

$$R_n = S_{\downarrow}(1-\alpha) + L_{\downarrow} + L_{\uparrow} \tag{9}$$

Where $S_{\downarrow}$ is incoming solar radiation (W m^{-2}), α is the snow-surface albedo, and $L_{\downarrow}$ and $L_{\uparrow}$ are incoming and outgoing longwave radiation (W m^{-2}), respectively. Incoming and outgoing energy flux terms were treated as positive and negative values, respectively.

[38] TOPORAD [*Dozier*, 1980; *Dozier and Frew*, 1990] was used to model hourly clear-sky incoming solar radiation for each 30-m pixel within each of the six modeling domains. Incoming solar radiation in the visible (0.3–0.9 um), near infrared (0.9–1.2 um) and middle infrared (0.9–1.2) was calculated separately and then integrated. To account for terrain illumination, clear-sky incoming solar radiation surfaces were used to downscale 1/2°-resolution incoming solar radiation data from the Geostationary Operational Environmental Satellites (GOES) [*Pinker and Laszlo*, 1992] to 30-m resolution:

$$S_{\downarrow} = \left(\left[\sum_{h=1}^{24} S_{t,h} \Big/ \sum_{h=1}^{24} \overline{S_{t,h}} \right] \sum_{h=1}^{24} S_{G,h} \right) /24 \tag{10}$$

Where $S_{\downarrow}$ is incoming solar radiation at 30-m resolution, $S_{t,h}$ is modeled clear-sky incoming solar radiation for hour h, $\overline{S_t}$ is the average incoming clear-sky solar radiation across the 16-km^2 modeling domain, and S_G is GOES-derived incoming solar radiation. To account for the effects of vegetation on incident shortwave radiation the result of (10) was multiplied by a nonlinear insolation transmission coefficient [*Cline and Carroll*, 1999]. To reduce computational expense, hourly values of S_t were simulated every 10 days and then interpolated linearly as a function of time between the 10-day intervals. Snow surface albedo was estimated using a snow-age-based decay function [*U.S. Army Corps of Engineers*, 1956].

[39] Using the spatially distributed air temperature estimates and relative humidity surfaces, we applied the Idso2 formulation [*Idso*, 1981] to model the spatial distribution of incoming longwave radiation [*Cline et al.*, 1998]. Specific humidity was calculated from relative humidity and temperature observations at the Center meteorological station. Spatial estimates of relative humidity were then derived from air temperature surfaces with specific humidity assumed spatially constant throughout the modeling domain [*Cline et al.*, 1998]. The effect of vegetation on incoming longwave radiation was accounted for by weighting emissivity as a function of forest cover density [*Cline and Carroll*, 1999].

5. Results

5.1. Field Surveys

[40] The mean snow depth at the six sites in April 2002 was 34% of that in April 2001, with variability also lower in 2001 (Table 3). Snow density was 25% greater in April 2001 than in 2002 (Table 3). The considerable formation of faceted snow grains may explain the lower density in 2002 as the density of faceted snow grains is typically lower than that of rounded snow grains.

[41] Mean snow depth at Slumgullion and Upper San Juan decreased by 77% and 60%, respectively, between the April 2001 and May 2001 snow surveys, with snow depth variability increasing (Tables 3 and 4). In 2002, snow depth decreased by 66% and 55% between the April and May snow surveys at the Slumgullion and Upper San Juan sites, respectively. Trends in snow density are viewed with caution given that the Federal Sampler was used to measure snow density in April, while snow pits were used in May. Further, only 4 snow density measurements were made at each site in May on average versus 18 in April (Tables 3 and 4). In all cases the variability in snow depth was greater than that of snow density.

[42] In April 2001 snow depths at Slumgullion, Wolf Creek Summit and Lily Pond were greater than the mean

Table 3. Summary of April 2001 and 2002 Snow Depth and Snow Density Measurements Made During the April 2001 and 2002 Field Campaigns[a]

	Slumgullion		Upper Rio Grande		Middle Creek		Upper San Juan		Wolf Creek Summit		Lily Pond	
	Density	Depth	Density	Depth	Density	Depth	Density	Depth	Density	Depth	Density	Depth
						2001						
Minimum	201	37	316	0	253	140	297	128	305	135	315	0
Maximum	341	193	401	141	382	357	456	380	407	335	455	176
Mean	287	119	355	63	344	201	378	246	343	260	385	106
CV	0.10	0.21	0.07	0.59	0.10	0.16	0.12	0.17	0.09	0.13	0.11	0.31
n	21	259	18	154	13	85	21	218	19	152	20	136
SNOTEL	284	160	370	55	366	201	355	244	357	268	402	113
						2002						
Minimum	162	0	222	0	194	0	219	0	195	0	209	0
Maximum	377	66	269	34	492	98	385	161	390	136	351	105
Mean	268	29	246	1	329	45	297	56	259	86	277	25
CV	0.19	0.55	0.13	5	0.23	0.47	0.19	0.57	0.16	0.27	0.17	0.96
n	25	203	2	141	20	134	17	211	19	129	11	136
SNOTEL	334	54	n/a	0	359	30	385	47	303	92	302	16

[a]Snow depth values are in cm, and snow density values are in kg m^{-3}. CV is coefficient of variation.

observed snow depth of the surrounding areas with snow depth at Slumgullion greater than one standard deviation above the mean (Figure 3a). Snow depths at Upper San Juan and Middle Creek were representative of the mean of the surrounding observations.

[43] Observed snow depths in April 2002 at Upper Rio Grande, Middle Creek and Upper San Juan were below the mean values (Figure 3b). Slumgullion and Wolf Creek Summit snow depths remained well above the mean (Figure 3b).

5.2. Binary Regression Trees

[44] Results of the cross-validation showed that regression tree snow depth models developed using the data collected at the Upper Rio Grande and Middle Creek sites were unstable. Instability was indicated by the absence of a minima in the plots of deviance versus number of terminal nodes [*Chambers and Hastie*, 1993]. Models developed using the May 2002 Slumgullion data set were also unstable. These instabilities likely existed because of small sample sizes and relatively homogeneous terrain.

[45] The relationship between snow depth and physiographic variables varied from 2001 to 2002 (Table 5). Elevation and solar radiation played the largest role in snow distribution in 2001 and 2002, respectively as indicated by the frequency and level of occurrence of these variables in the regression tree models (e.g., Figure 4). Elevation played the dominant role in controlling snow distribution in

Table 4. Summary of May 2001 and 2002 Snow Depth and Snow Density Measurements[a]

	2001				2002			
	Slumgullion		Upper San Juan		Slumgullion		Upper San Juan	
	Density	Depth	Density	Depth	Density	Depth	Density	Depth
Minimum	337	0	422	30	294	0	289	0
Maximum	363	78	481	218	388	75	453	109
Mean	350	28	461	98	341	10	363	25
CV	0.04	0.82	0.05	0.49	0.19	1.50	0.22	1.28
n	4	49	6	76	2	45	4	72

[a]Snow depth values are in cm, and snow density values are in kg m^{-3}. CV is coefficient of variation.

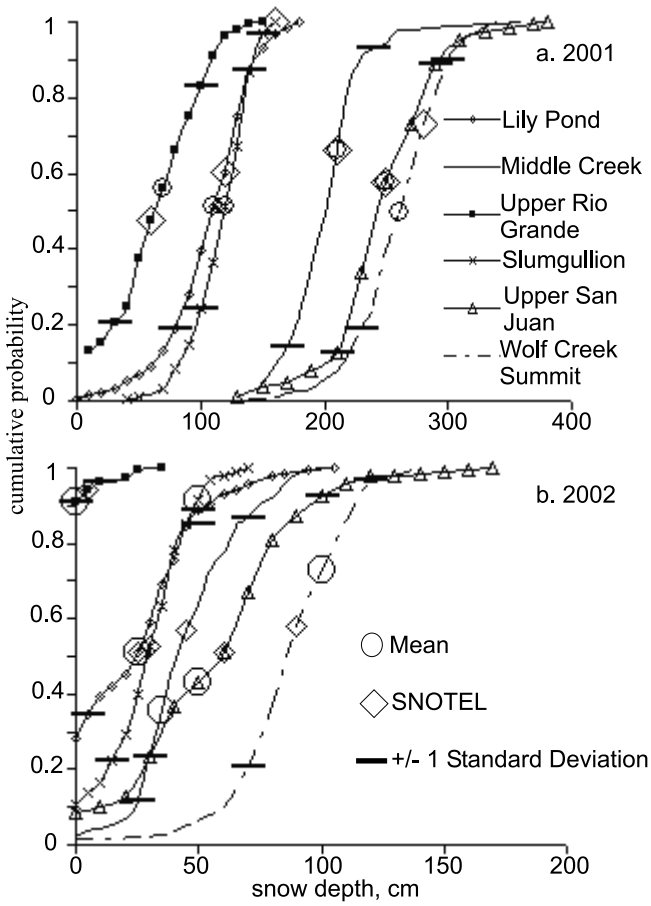

Figure 3. Statistical distribution of snow depth measurements surrounding the SNOTEL sites in April (a) 2001 and (b) 2002.

Table 5. Regression Tree Snow Depth Model Summary[a]

	Terminal Nodes		Additional Variables		R^2	
	2001	2002	2001	2002	2001	2002
			April			
Slumgullion	9	8	Sx, slope, aspect	slope, aspect	0.62	0.42
Upper San Juan	9	10	Sx	fca, slope	0.57	0.66
Wolf Creek Summit	9	6	Sx, fca	Sx	0.64	0.60
Lily Pond	6	8	slope, aspect	Sx, fca	0.47	0.50
			May			
Slumgullion	5	n/a	none	n/a	0.69	n/a
Upper San Juan	7	6	Sx, fca	Sx, fca	0.77	0.75

[a]Note all models included elevation (m) and solar radiation (W m^{-2}). Regression tree models developed for the Middle Creek and Upper Rio Grande data sets were unstable and are not shown. Maximum upwind slope (degrees), *Sx*, is designed to represent the effect of wind on snow redistribution. Slope and aspect are in degrees and forest-covered area, fca, is in percent. R^2 is the coefficient of determination for the regression tree model.

4 out of 5 cases in 2001, with solar radiation dominant in all cases in 2002 (Table 6).

[46] Average modeled SWE was significantly lower than that measured at the Slumgullion SNOTEL site (Figures 5a and 5b). In April 2001 observed snow depth at Upper San Juan was fairly representative of the mean regression-tree-modeled snow depth. However, snow density was positively correlated ($p = 0.0004$) with solar radiation (slope = 1.94) and thus SWE did not exhibit the same spatial pattern as snow depth. Rather, observed SWE at Upper San Juan was significantly greater than the mean of the grid element (Figure 5a). In April 2002 – where mean observed (Figure 3b) and modeled snow depths were less than the SNOTEL value – SWE was quite representative of the mean SWE of the surrounding grid element (Figure 5b); snow density was significantly ($p = 0.007$) correlated with elevation (slope = −0.28), forest covered area (slope = −2.59), and a cosine transformation of aspect (slope = 0.2017) and therefore SWE distribution was not identical to snow depth distribution. Observed SWE at Wolf Creek Summit in April 2001 and 2002 was considerably greater than the mean SWE of the surrounding grid element (Figures 5a and 5b).

[47] In April 2001 observed SWE at Lily Pond was substantially greater than the 16- and 4-km^2 grid element mean values (Figure 5a). This was due to the strong influence of elevation in the regression tree snow depth model, where snow depth decreased at lower elevations. Given that this site is located on the top of a plateau, with an extent of approximately 1 km^2 (Figure 1), it is intuitive that SNOTEL SWE was more representative of the 1-km^2 grid element (Figure 5a). In April 2002, the dominance of solar radiation in the regression tree model (Table 6) resulted in greater predicted snow depths on the north facing slopes to the north of the plateau on which the SNOTEL site resides. Hence SWE at Lily Pond was significantly below the mean of the 4- and 1-km^2 grid elements. Solar radiation played a more important role in the April 2002 regression tree model, with snow depth decreasing with increasing solar radiation. Solar radiation at Lily Pond was more representative of the mean solar radiation over the surrounding 16 km^2 grid element.

[48] At Slumgullion, 52 pixels, out of a possible 17,689 within the 16 km^2 area, were identified as satisfying the criteria for optimality (Figure 6a). The cumulative absolute deviance from the mean modeled snow depth of these pixels was only 0.61 cm for the two April model simulations. Of those 52 pixels, 20 overlapping or immediately adjacent pixels had a mean absolute deviance of less than 3 cm for the April and May simulations. The location of the SNOTEL site was not considered optimal because it is situated on a north facing slope and therefore is exposed to less radiation than areas within the optimal terminal node of the regression tree model (Table 7). Here we refer to the optimal terminal node as the terminal node with a snow depth value closest to the mean predicted snow depth value over the modeling domain.

[49] In April 2001 the physiographic conditions at the Upper San Juan SNOTEL site met the constraints of the optimal terminal node. Upper San Juan was not located optimally in April 2002 because solar radiation played a more important role in snow distribution in 2002 (Table 6); the site is located in an area with relatively high incident solar radiation (Table 7).

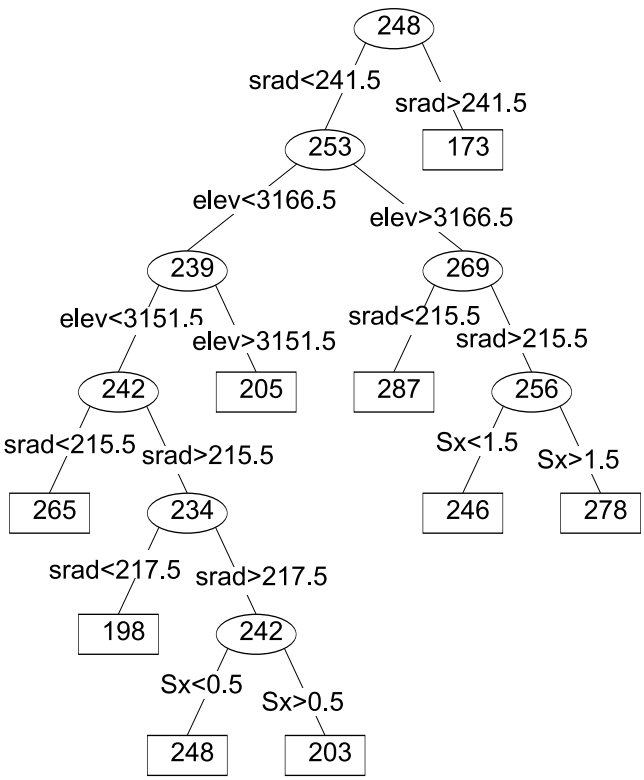

Figure 4. Regression tree snow depth model for the Upper San Juan study area in April 2001. The values in the ellipsoidal and rectangular nodes are the mean snow depth values (cm) of all samples satisfying the splitting criteria for that node. Ellipsoidal nodes are root nodes and rectangular nodes are terminal nodes. The solar radiation index, srad (W m^{-2}), is a summation of the daily integrated solar radiation surfaces from 15 November to 15 April. The maximum upwind slope, *Sx* (degrees), is a terrain-based parameter designed to represent the variability in snow deposition as a result of wind redistribution. Elevation (m) is abbreviated as "elev."

Table 6. Frequency of Appearance of Physiographic Variables at Different Levels in the Regression Tree Snow Depth Models for April 2001 and 2002[a]

	Solar Radiation, W m^{-2}		Elevation, m		S_x, deg		fca, %		Slope, deg		Aspect, deg	
Tree Level	2001	2002	2001	2002	2001	2002	2001	2002	2001	2002	2001	2002
1	1	5	4	0	0	0	0	0	0	0	0	0
2	3	0	2	4	1	0	0	3	0	0	1	1
3	2	2	3	2	1	0	0	2	2	1	0	1
4	1	1	1	2	2	2	1	1	1	1	0	1
5	1	0	1	2	0	1	1	1	0	1	1	0
6	0	0	1	0	1	0	0	0	0	0	0	0

[a]For example, a value of 2 for tree level 4 indicates that the specified variable appeared in the fourth level in two of the eight models for that year. S_x is maximum upwind slope, and fca is forest-covered area.

[50] At Wolf Creek Summit, April 2001 and 2002 optimal terminal nodes did not overlap in space. However, the second most optimal terminal node (i.e., the second closest to the mean) in April 2001 did overlap with the optimal terminal node of April 2002. The physiographic attributes at Wolf Creek Summit met the criteria of the common optimal terminal node (Figure 6c and Table 7). This was the only site that met these criteria.

[51] At Lily Pond only 26 pixels satisfied the criteria for optimality. Because of the low elevation and slope at the SNOTEL site relative the surrounding area, the site was not within the optimal area (Table 7). In 2001, a level three regression-tree-model split on slope meant the difference between the optimal terminal node and a value 56% greater than the mean snow depth. In 2002, a fifth-level split on elevation meant the difference between optimality and a value 59% below the optimal node; increased elevation resulted in decreased snow depth.

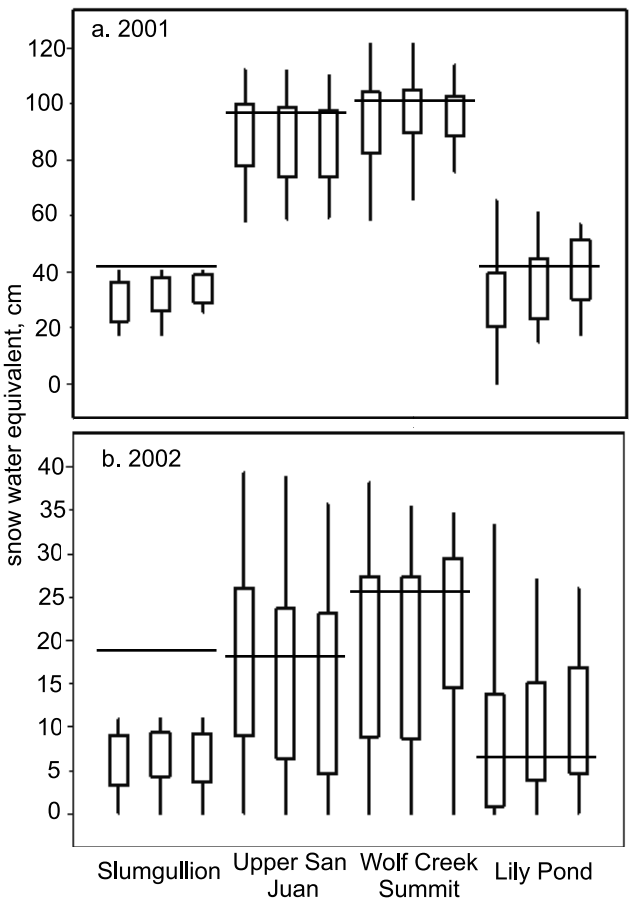

Figure 5. Statistical distribution of modeled snow water equivalent for April (a) 2001 and (b) 2002. Results for 16-, 4-, and 1-km^2 grid elements are shown from left to right, respectively. Measured snow depth at the SNOTEL stations is indicated by the horizontal hash marks. Vertical lines represent the range of modeled values and rectangles indicate values within plus or minus one standard deviation of the mean. Results for the Upper Rio Grande and Middle Creek sites are not shown because regression tree models were unstable.

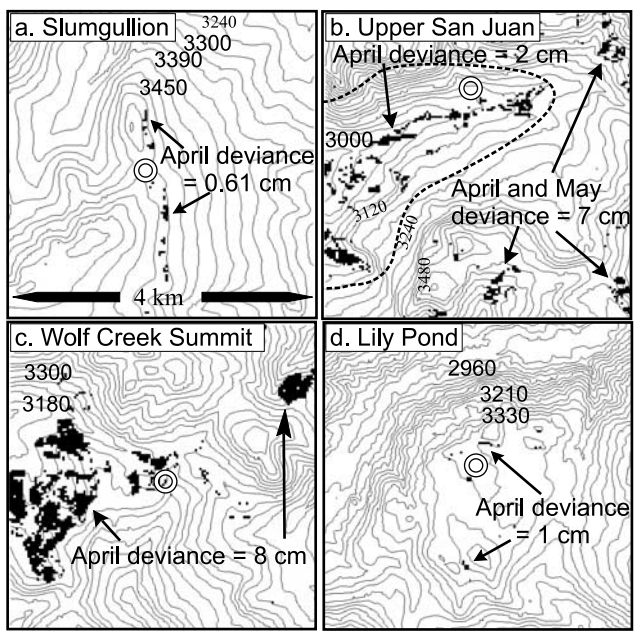

Figure 6. Optimal areas for measuring mean grid element snow depth at the (a) Slumgullion, (b) Upper San Juan, (c) Wolf Creek Summit, and (d) Lily Pond study areas. These areas, shaded in black, had the lowest cumulative absolute deviance from the mean modeled snow depth. White rings indicate SNOTEL site locations (not to scale). Areas enclosed by the dotted line in Figure 6b had an April deviance of 2 cm. The Wolf Creek Summit site was within the optimal area.

Table 7. Range of Physiographic Attributes at Optimal Site Locations Compared to Values at SNOTEL Sites[a]

	Slumgullion			Upper San Juan			Wolf Creek Summit			Lily Pond		
	Minimum	Maximum	SNOTEL	Minimum	Maximum	SNOTEL	Minimum	Maximum	SNOTEL	Minimum	Maximum	SNOTEL
Solar radiation, W m^{-2}	**218**	**226**	**215**	**218**	**223**	**227**	181	222	210	225	239	228
Elevation, m	3514	3530	3518	2935	3152	3089	3210	3333	3331	**3356**	**3369**	**3375**
Sx, degrees	4	26	13	−21	0	−3	−23	3	−4	−3	9	−3
Vegetation density, %	0	62	45	0	82	3	0	60	46	0	64	43
Slope, degrees	8	25	9	1	31	6	0	33	15	**9**	**31**	**3**
Aspect, degrees	**83**	**91**	**65**	**220**	**352**	**195**	0[b]	360[b]	322	164	244	200

[a]Bold values indicate that SNOTEL variable value is outside the range of values at the optimal site location.
[b]Ninety-five percent of values were between 240° and 360°.

[52] Of the four sites considered, less than 2.4% of each grid element, on average, satisfied the physiographic criteria of optimality for future observations.

5.3. Snow Water Equivalent Reconstruction

[53] Estimates of SWE distribution using the reconstruction model adequately matched regression tree model results (Figures 7a and 7b). Both models predicted a band of relatively lower SWE accumulation that extends from the northwest corner of the Wolf Creek Summit grid element to the southeast. Similarly, high SWE accumulation was simulated in the southern and northeast portions of the grid element. The reconstruction model did, however, have a greater range in values. Over the six 16-km^2 grid elements, mean reconstructed SWE deviated from the mean regression tree model derived SWE by 8% on average.

[54] Figures 8a–8f shows the empirical cumulative distribution (ECD) plots for SWE throughout the 2002 snowmelt season. As the snowmelt season progresses the ECD shifts toward the y axis. As SCA decreases the y intercept of the ECD increases; subtracting the y intercept from 1 gives the fractional SCA over the modeling domain. In some cases SNOTEL SWE began the melt season with an empirical cumulative probability of 0.4 to 0.6 indicating a sufficient representation of mean SWE (Figures 8b, 8d, and 8f). Later in the snowmelt season SNOTEL SWE values fell lower in the distribution (Figures 8b, 8d, and 8f), indicating that snowmelt rates at these SNOTEL sites were greater than the average melt rate over the surrounding 16 km^2 grid element. At the beginning of the snowmelt season relationships between reconstructed SWE and point SNOTEL SWE (Figures 8a–8f) were consistent with relationships between regression tree SWE estimates and SNOTEL SWE (Figure 5). This was true for May as well (not shown). Snow water equivalent at Wolf Creek Summit began the 2002 snowmelt season with a SWE value within 1 standard deviation of the 16-km^2 mean (Figure 5b) but dramatically overestimated the 16-km^2 mean throughout most of the snowmelt season (Figure 8e); snowmelt rates at the SNOTEL site were lower than the average melt rate over the surrounding 16 km^2 grid element.

[55] The 2001 temporal trends in SNOTEL SWE representativeness at the Slumgullion site were relatively consistent at the 16-, 4-, and 1-km^2 scales (Figure 9). Temporal trends in SWE representativeness were also consistent across the 3 different scales at the Wolf Creek Summit and Upper Rio Grande sites (not shown). Early in the 2001 snowmelt season, SWE overestimates at the Upper San Juan site were greatest relative to the surrounding 1-km^2 grid element (Figure 9); SNOTEL SWE empirical cumulative probability values increased at the 1-km^2 scale relative to the 4- and 16-km^2 scales. Temporal trends in representativeness at the Middle Creek and Lily Pond sites also exhibited some sensitivity to scale, with the greatest SNOTEL SWE cumulative probability values occurring at the 1-km^2 scale (not shown). Temporal trends in SWE representativeness at different scales were similar in 2002; the Upper San Juan and Lily Pond sites were sensitive to scale.

[56] Negative correlations between the scaling coefficient and accumulated degree days were widespread (Figures 10a–10f). Positive correlations were found in areas with persistent snow cover. Unlike areas with negative correlations, these areas provide information about the SWE over the study domain throughout the snowmelt season and were therefore considered optimal for future observations. Areas with correlations above 0.73 were restricted to relatively steep north facing slopes (Figures 10a–10f). Correlations at the 16-km^2 scale surrounding Slumgullion were fairly consistent in 2001 and 2002 (Figures 11a and 11b). Other sites also showed repeating spatial patterns of correlations during the two years (not shown).

[57] At Upper San Juan correlations increased with decreasing scale (Figure 12); variability in snow cover duration decreased at smaller scales. At other sites correla-

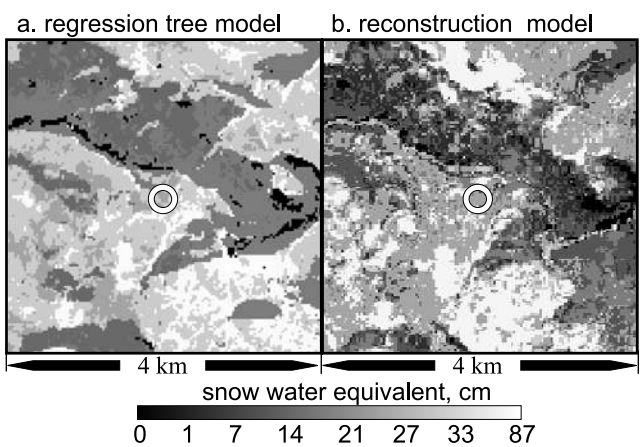

Figure 7. Modeled snow water equivalent (cm) distribution at the Wolf Creek Summit study area on 4 April 2002 using (a) a regression tree model and (b) the net radiation/temperature index reconstruction model. SNOTEL site location is indicated by the white ring.

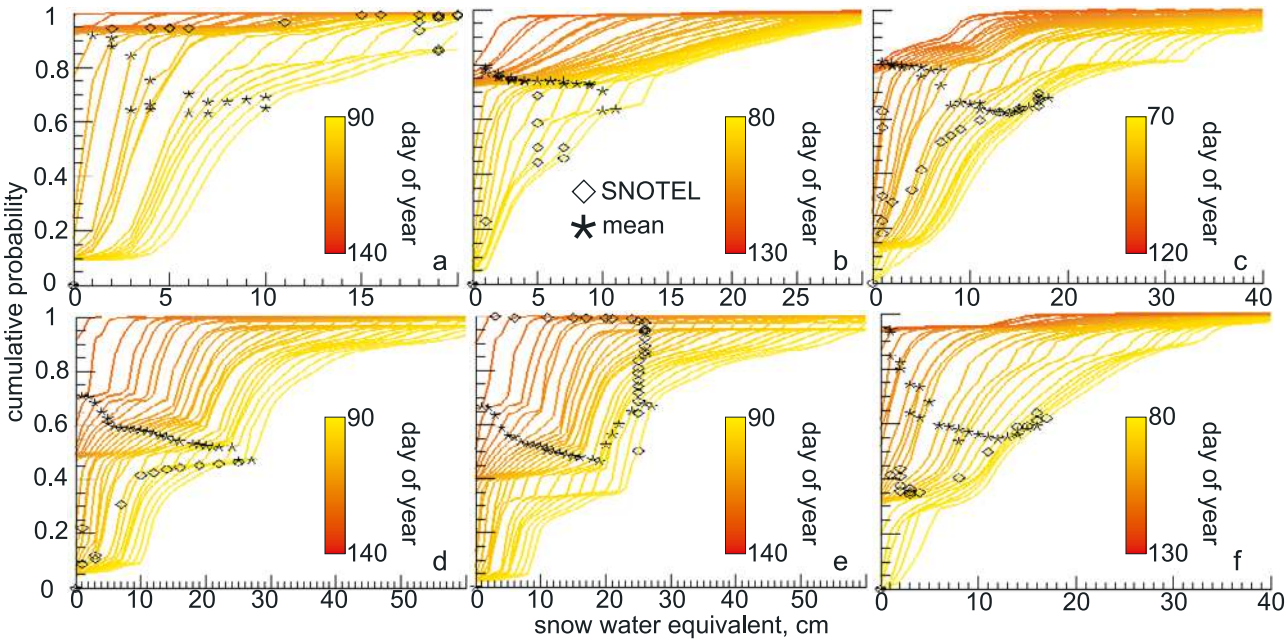

Figure 8. Empirical cumulative distribution functions of modeled snow water equivalent during the 2002 snowmelt season over the 16-km^2 grid element surrounding (a) Slumgullion, (b) Upper Rio Grande, (c) Middle Creek, (d) Upper San Juan, (e) Wolf Creek Summit, and (f) Lily Pond. Plots are shown for every 2 days. Mean grid element and SNOTEL-observed snow water equivalent values are indicated for each day of year.

tions either stayed constant with scale or increased as scale decreased.

6. Discussion

[58] Small-scale variability in snow distribution cannot be resolved if the distance between observations is greater than the correlation length scale [*Blöschl*, 1999]. Clearly, the spacing of SNOTEL stations is too large to resolve this small-scale variability. We used nonlinear snow distribution and mass balance models to estimate the small-scale variability around SNOTEL sites, leaving the task of estimating large-scale variability in SWE to complimentary work using remote sensing [*Chang et al.*, 1991; *Chang and Rango*,

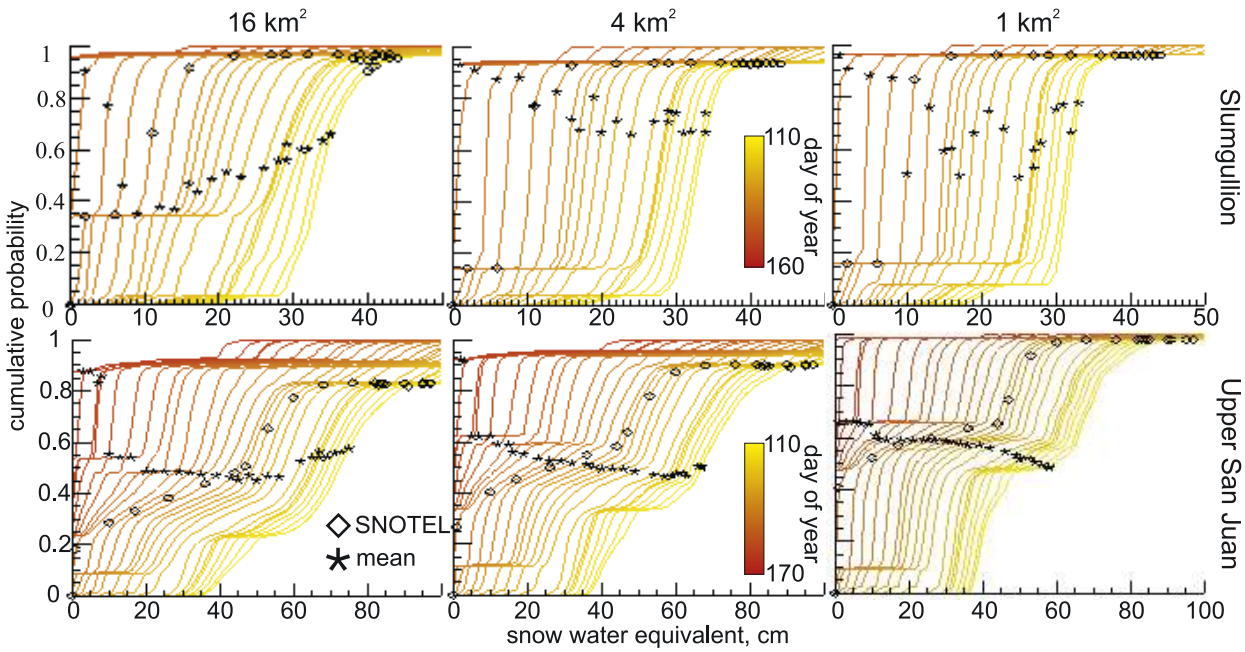

Figure 9. As in Figure 8 but for Slumgullion and Upper San Juan during the 2001 snowmelt season and for the 16-, 4-, and 1-km^2 grid elements.

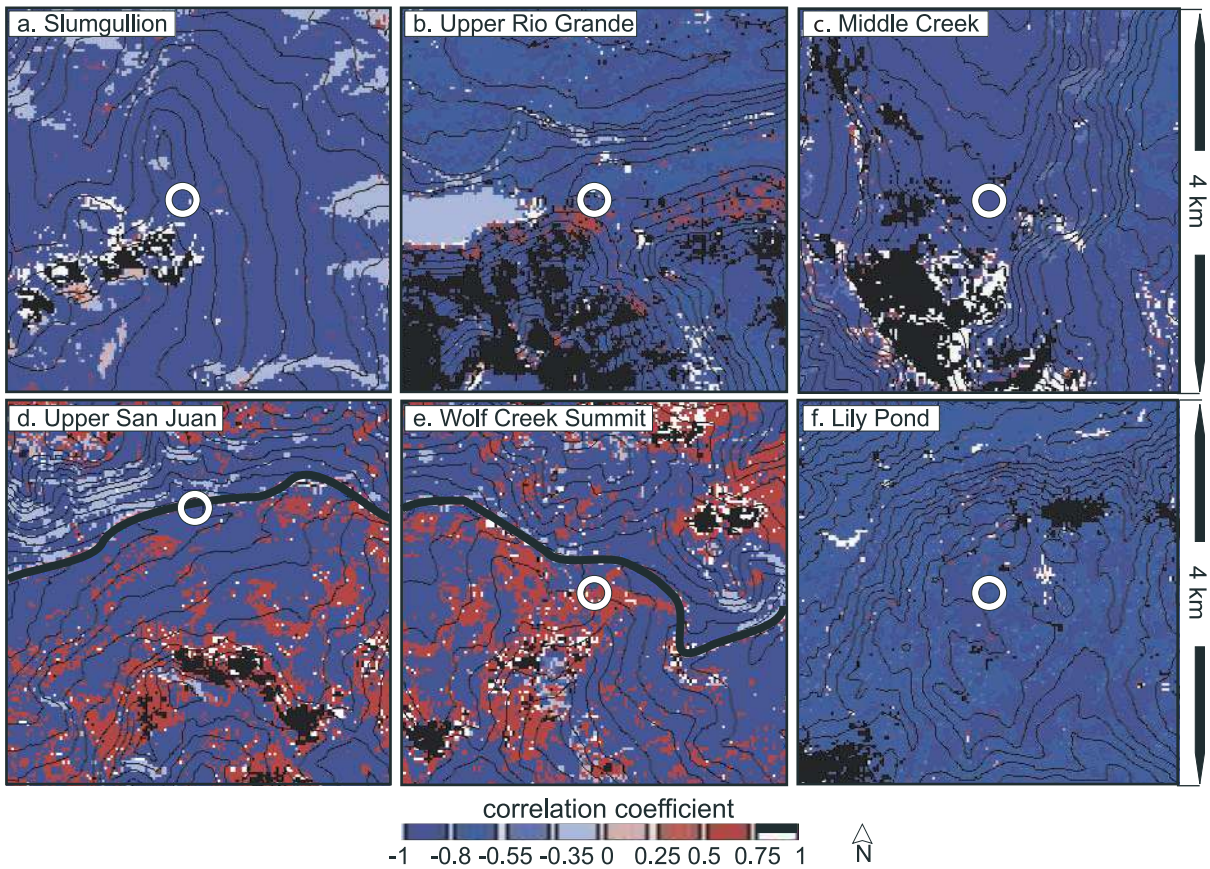

Figure 10. The spatial distribution of correlation coefficients between scaling coefficients and accumulated degree days for the 2002 snowmelt season at (a) Slumgullion, (b) Upper Rio Grande, (c) Middle Creek, (d) Upper San Juan, (e) Wolf Creek Summit, and (f) Lily Pond. SNOTEL site locations are indicated by the white rings. Areas in black had correlations above 0.73 during the 2001 and 2002 snowmelt seasons and are considered optimal for future automated observation systems. U.S. Highway 160 is shown in Figures 10d and 10e.

2000; *Foster et al.*, 1991] and modeling [*Carroll et al.*, 2001; *Martinec*, 1991; *Rango*, 1988]. The relatively coarse resolution (or support, as termed by *Blöschl* [1999]) of these SWE estimation techniques cannot resolve small-scale SWE variability and therefore this variability is smoothed out across the grid element scale [*Blöschl*, 1999]. Hence evaluation of these remotely sensed and model estimates has relied on the ability of ground observations to represent the average conditions of subgrid element variability. The work presented here has shown that SNOTEL observations do not adequately represent average grid element SWE. Further, we have improved the ability to scale these data to grid elements and enhanced the utility of these six SNOTEL stations for evaluating larger-scale remote sensing and modeling approaches by defining the subgrid element SWE variability. We assert that the approach outlined in this research is transferable to other sites. We do not assert that these results are transferable to other SNOTEL sites, nor are we suggesting that SNOTEL stations be moved or that our site selection criteria are suitable for the needs of empirical water supply forecasts.

[59] As an example application of our results, we evaluated the 1-km^2 resolution SWE product generated by the National Operational Hydrologic Remote Sensing Center (NOHRSC) [*Carroll et al.*, 2001]. NOHRSC evaluates residuals between observed SNOTEL SWE and their 1-km^2 modeled SWE estimates on a daily basis. On the basis of the magnitude of these residuals, a decision is made

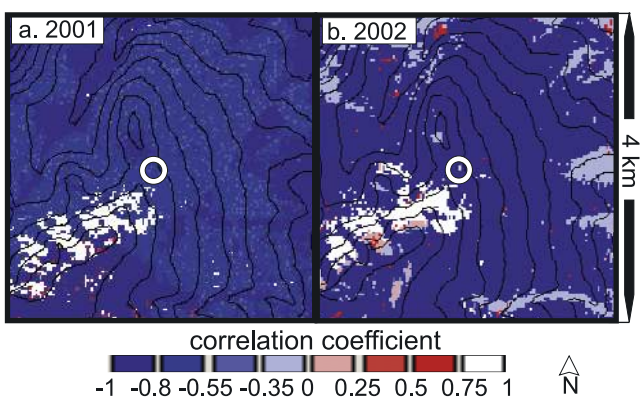

Figure 11. As in Figure 10 but for Slumgullion during the (a) 2001 and (b) 2002 snowmelt seasons. Note the lack of interannual variability in the distribution of the correlation coefficients.

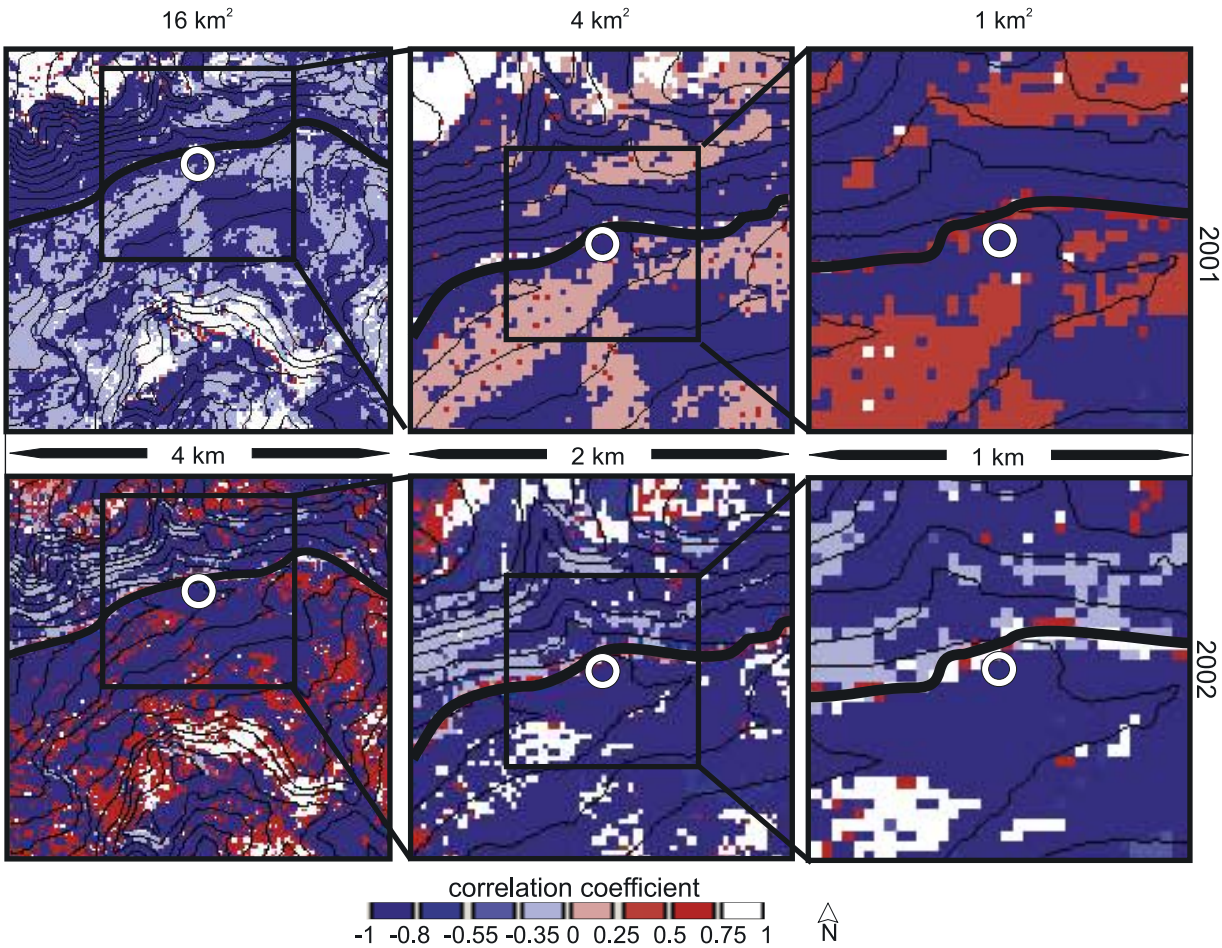

Figure 12. As in Figure 10 but for the Upper San Juan site during the 2001 and 2002 snowmelt seasons. Correlations are shown for the 16-, 4-, and 1-km^2 grid elements. Note the increased correlations at smaller scales.

as to whether or not modeled SWE will be updated to the observed value. At Upper San Juan in 2004, NOHRSC updated modeled SWE several times throughout the snowmelt season as the observed melt at the SNOTEL site was considerably greater than their model predicted (Figure 13). The research presented here, although undertaken during 2001 and 2002, has shown that the melt rate at Upper San Juan is consistently greater than the surrounding 1-km^2 (Figure 9). SWE residuals were not as great at Wolf Creek Summit (Figure 13); we have shown that the snowmelt rate surrounding Wolf Creek Summit is less than that of the surrounding 16 km^2 (Figure 8e). These comparisons indicate that the NOHRSC model may actually be representing the system more accurately than would be concluded using the SNOTEL data alone.

[60] The six SNOTEL sites studied here are the primary source of ground-based SWE data within the study areas of many of the aforementioned, larger scale, complimentary efforts [*Brubaker and Menoes*, 2001; *Chang et al.*, 1991; *Rango and Martinec*, 1982; *Shafer et al.*, 1979]. The implications of this work should inspire similar investigations, as a common resolution (or support) between snow pillows (~2-m support), remotely sensed SWE observations (e.g., 25-km^2 resolution), and model grid elements (e.g., 1-km^2 resolution) may be far from fruition. These future efforts should focus on the development of ground-based observation networks that represent the continuum of SWE distribution within their surrounding grid elements. Interseasonal variability exists due to the aforementioned differences between accumulation and ablation season snowpack processes. Thus it is particularly difficult to identify an observation location that represents both accumulation and ablation season processes; locations that provide snowpack information throughout the snowmelt season (Figure 10) are in areas with above average SWE accumulation (Figure 7). We have identified optimal locations for these distinctly different seasons (Figures 6 and 10), however, these optimal locations do not overlap in space. Thus future observations may need to be located with the specific objective of representing either accumulation or ablation season processes.

[61] It is particularly challenging to capture the variability in factors that control snow distribution in forested environments (e.g., the influence of vegetation on the spatial distribution of solar radiation, interception of snowfall, sublimation, longwave radiation emission, and wind field patterns). Of the previously attempted work with regression tree snow distribution models [*Anderton et al.*, 2004; *Balk and Elder*, 2000; *Elder*, 1995; *Elder et al.*, 1998; *Erxleben et al.*, 2002; *Molotch et al.*, 2005; *Winstral et al.*, 2002],

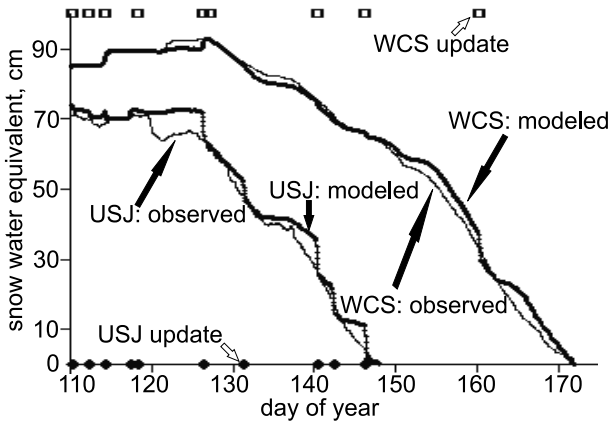

Figure 13. Modeled snow water equivalent (from the National Operational Hydrologic Remote Sensing Center) over the 1-km^2 grid element surrounding the Wolf Creek Summit (WCS) and Upper San Juan (USJ) SNOTEL sites. Observed SNOTEL snow water equivalent is also shown. Squares across the top of the view graph indicate time steps when the model was updated to match WCS observations. Diamonds across the bottom of the view graph indicate time steps when the model was updated to match USJ observations. Note the relatively rapid deviation between modeled grid element SWE and observed SWE at USJ. Data source is National Operational Hydrologic Remote Sensing Center (http://www.nohrsc.noaa.gov/).

only the work of *Erxleben et al.* [2002] and *Elder et al.* [1998] were performed in areas with considerable forest cover. The explanatory ability (average $R^2 = 0.56$) of the regression tree models developed here were encouraging relative to these two previous works (average R^2 values of 0.25 and 0.6, respectively). This research relies on the statistical relationships represented by the regression tree models to define the continuum of snow distribution over an areal extent that exceeds the extent observed. It is important to note that the relationships between snow depth and independent variables can change over a few kilometers [*Elder*, 1995]. We used as many observations as possible, over as large an extent as possible, while trying to maintain a sufficient sampling density to ensure satisfactory model development.

[62] As found here, previous work [*Anderton et al.*, 2004] has noted an increased correlation between snow depth and solar radiation during water years with relatively lower snow accumulation. The dominance of orographics in the above average snow accumulation year (i.e., 2001) may have caused stronger correlations with elevation. In 2002, a greater proportion of the total SWE accumulation may have melted or sublimated before the April snow survey, increasing correlations with solar radiation; radiative fluxes tend to dominate snowmelt fluxes early in the snowmelt season [*Molotch et al.*, 2004a]. In April 2002 the snow accumulation season ended about two weeks before the snow survey. The shift in dominance from elevation to solar radiation from 2001 to 2002 significantly impacted the representativeness at Lily Pond (Figures 5a and 5b).

[63] The relatively short duration of the snowmelt season and the presence of cloud cover, which prevented detection of SCA, resulted in less favorable results than previous applications of the SWE reconstruction technique [*Cline et al.*, 1998; *Molotch et al.*, 2004a]. At times, the combination of these issues resulted in significant changes in SCA (e.g., large areas became snow-free) with out the intermediate observations of SCA needed to observe depletion rates. Hence the application of this technique may be more challenging in continental regions where the snowpack is relatively shallow.

[64] Application of this technique is also challenging in forested environments where accurate detection of fractional SCA is more difficult due to diminished viewable gap fractions [*Liu et al.*, 2004] and because the spectral unmixing algorithm has difficulty separating the spectra of dirty snow from snow-free end-members [*Rosenthal and Dozier*, 1996]. Furthermore, we currently lack the ability to detect snow cover properties beneath the canopy. We assumed that pixel-specific under-canopy fractional SCA was equal to the SCA detected within the viewable gap fraction. There are inherent limitations to this assumption given that snow distribution is not uniform due to interception of snowfall and vegetation-induced variability in snowmelt and sublimation rates.

[65] *Sicart et al.* [2004] showed that daily net radiation increases with decreasing canopy density, particularly at lower latitudes (i.e., increased solar elevation) and when snow-surface albedo is low (i.e., 0.5). In our simulations net radiation increased with decreasing canopy density; relatively low snow albedo (minimum albedo = 0.55) and high solar elevations were present during the snowmelt seasons.

[66] The accuracy of the modeled turbulent flux contribution to snowmelt depends largely on the degree day coefficient. The degree day coefficient calculated here (i.e., 0.15 cm $°C^{-1}$ d^{-1}) seems reasonable relative to the 0.20 value previously found at Sleepers River [*Brubaker et al.*, 1996] and the 0.17 value found at Weissfluhjoch [*Kustas et al.*, 1994]; relative humidity and therefore the degree day coefficient is lower in our continental study region.

[67] Future research efforts will be devoted toward applying these techniques at other SNOTEL sites throughout the western United States, conducting thorough comparisons with coarser-scale modeling results (e.g., 4-km resolution), and exploring the use of other variables (e.g., net radiation) for predicting scaling coefficients.

7. Conclusion

[68] At maximum accumulation differences between observed SWE at SNOTEL sites and the mean SWE of the surrounding areas were not consistent from site to site. However these differences were fairly consistent in 2001 and 2002. On average, less than 2.4% of each grid element satisfied the physiographic criteria of optimality for future observations of accumulation season dynamics. Temporal trends in SWE representativeness did not exhibit significant variability between the two years studied. Steep, north facing slopes with relatively persistent snow cover were determined to be optimal locations for observing SWE during the ablation season. These locations did not overlap in space with the accumulation-season-optimal locations and therefore future observations may need to be placed with the specific objective of representing either accumula-

tion or ablation season processes. This research has shown that SNOTEL SWE data are generally unrepresentative of mean grid element SWE. The consistency in the relationship between mean grid element SWE and SNOTEL SWE during these two different water years makes these results particularly useful for large-scale SWE variability studies that require ground observations for evaluation, initialization or calibration purposes. Furthermore, these consistencies have implications for future observation network design in that results from short-term studies (e.g., 2 years) can be used to design long-term observation networks.

[69] **Acknowledgments.** R. Brice, T. Bardsley, R. Davis, W. Rosenthal, S. Fassnacht, T. Pagano, K. Dressler, J. Hamblen, D. Lampkin, J. Dozier, C. McKenzie, S. Leake, A. Winstral, K. Elder, D. Pitcher, K. Naggy, A. Hobson, J. McConnell, D. Boyle, S. Markstrom, R. Viger, T. Painter, B. Getz, M. Gillespie, and others are all thanked for technical and field support. This research was supported by the Cooperative Institute for Research in Environmental Sciences (CIRES) Visiting Fellows Program. Data collection was supported by SAHRA (Sustainability of Semi-Arid Hydrology and Riparian Areas) under the STC Program of the National Science Foundation, agreement EAR-9876800. Additional support was provided by the Climate Assessment for the Southwest (CLIMAS), Institute for the Study of Planet Earth. Francesca Pellicciotti, Shirley Kurk, and one anonymous reviewer are thanked for comments that improved this manuscript.

References

Anderton, S. P., S. M. White, and B. Alvera (2004), Evaluation of spatial variability in snow water equivalent for a high mountain catchment, *Hydrol. Processes*, *18*, 435–453.

Balk, B., and K. Elder (2000), Combining binary decision tree and geostatistical methods to estimate snow distribution in a mountain watershed, *Water Resour. Res.*, *36*, 13–26.

Beven, K. (1995), Linking parameters across scales: Subgrid parameterizations and scale dependent hydrological models, *Hydrol. Processes*, *9*, 507–525.

Blöschl, G. (1999), Scaling issues in snow hydrology, *Hydrol. Processes*, *13*, 2149–2175.

Brubaker, K. A., and M. Menoes (2001), A technique to estimate snow depletion curves from time-series data using the beta distribution, *Proc. East. Snow Conf.*, *58*, 343–346.

Brubaker, K., A. Rango, and W. Kustas (1996), Incorporating radiation inputs into the snowmelt runoff model, *Hydrol. Processes*, *10*, 1329–1343.

Carroll, T. R., D. W. Cline, G. Fall, A. Nilsson, L. Li, and A. Rost (2001), NOHRSC operations and the simulation of snow cover properties for the coterminous U.S., *Proc. West. Snow Conf.*, *69*, 1–14.

Chambers, J., and T. Hastie (1993), *Statistical Models in S*, 608 pp., CRC Press, Boca Raton, Fla.

Chang, A. T. C., and A. Rango (2000), Algorithm theoretical basis document for the AMSR-E snow water equivalent algorithm, version 3.1., report, NASA Goddard Space Flight Cent., Greenbelt, Md.

Chang, A., J. Foster, and A. Rango (1991), Utilization of surface cover composition to improve the microwave determination of snow water equivalent in a mountain basin, *Int. J. Remote Sens.*, *12*, 2311–2319.

Cline, D. (1997), Snow surface energy exchanges and snowmelt at a continental, midlatitude Alpine site, *Water Resour. Res.*, *33*, 689–702.

Cline, D. W., and T. R. Carroll (1999), Inference of snow cover beneath obscuring clouds using optical remote sensing and a distributed snow energy and mass balance model, *J. Geophys. Res.*, *104*, 19,631–19,644.

Cline, D. W., R. C. Bales, and J. Dozier (1998), Estimating the spatial distribution of snow in mountain basins using remote sensing and energy balance modeling, *Water Resour. Res.*, *34*, 1275–1285.

Consortium of Universities for the Advancement of Hydrologic Science Inc. (2003), A national center for hydrologic synthesis: Scientific objectives, structure, and implementation, *Tech. Rep. 5*, Santa Barbara, Calif.

Daly, C., R. P. Neilson, and D. L. Phillips (1994), A statistical topographic model for mapping climatological precipitation over mountainous terrain, *J. Appl. Meteorol.*, *33*, 140–158.

Dozier, J. (1980), A clear-sky spectral solar radiation model for snow-covered mountainous terrain, *Water Resour. Res.*, *16*, 709–718.

Dozier, J., and J. Frew (1990), Rapid calculation of terrain parameters for radiation modeling from digital elevation data, *IEEE Trans. Geosci. Remote Sens.*, *28*, 963–969.

Elder, K. (1995), Snow distribution in alpine watersheds, Ph.D. thesis, 309 pp., Univ. of Calif., Santa Barbara.

Elder, K., W. Rosenthal, and R. Davis (1998), Estimating the spatial distribution of snow water equivalence in a montane watershed, *Hydrol. Processes*, *12*, 1793–1808.

Erxleben, J., K. Elder, and R. Davis (2002), Comparison of spatial interpolation methods for estimating snow distribution in the Colorado Rocky Mountains, *Hydrol. Processes*, *16*, 3627–3649.

Fassnacht, S.R., K.D. Dressler, and R.C. Bales (2003), Snow water equivalent interpolation for the Colorado River Basin from snow telemetry (SNOTEL) data, *Water Resour. Res.*, *39*(8), 1208, doi:10.1029/2002WR001512.

Foster, J., A. Chang, D. Hall, and A. Rango (1991), Derivation of snow water equivalent in boreal forests using microwave radiometry, *Arctic*, *44*, 147–152.

GEWEX America's Prediction Project (2003), Report from the "hydrologic sciences" breakout session at the GAPP Mountain Hydrology Workshop, Seattle, Wash.

Gray, D., and D. Male (1981), *Handbook of Snow*, 776 pp., Elsevier, New York.

Idso, S. B. (1981), A set of equations for full spectrum and 8- to 14-um and 10.5- to 12.5-um thermal radiation from cloudless skies, *Water Resour. Res.*, *17*, 295–304.

Kustas, W. P., A. Rango, and R. Uijlenhoet (1994), A simple energy budget algorithm for the snowmelt runoff model, *Water Resour. Res.*, *30*, 1515–1527.

Liston, G. E. (1999), Interrelationships among snow distribution, snowmelt, and snow cover depletion: Implications for atmospheric, hydrologic, and ecologic modeling, *J. Appl. Meteorol.*, *38*, 1474–1487.

Liu, J., R. A. Melloh, C. E. Woodcock, R. E. Davis, and E. Ochs (2004), The effect of viewing geometry and topography on viewable gap fractions through forest canopies, *Hydrol. Processes*, *18*, 3595–3607.

Marks, D., and J. Dozier (1992), Climate and energy exchange at the snow surface in the alpine region of the Sierra Nevada: 2. Snow cover energy balance, *Water Resour. Res.*, *28*, 3043–3054.

Martinec, J. (1991), Areal modelling of snow water equivalent based on remote sensing techniques, in *Snow, Hydrology and Forests in High Alpine Areas: Proceedings of the Vienna Symposium*, *IAHS Publ.*, *205*, 121–129.

Molotch, N. P., T. H. Painter, R. C. Bales, and J. Dozier (2004a), Incorporating remotely sensed snow albedo into a spatially distributed snowmelt model, *Geophys. Res. Lett.*, *31*, L03501, doi:10.1029/2003GL019063.

Molotch, N. P., S. R. Fassnacht, R. C. Bales, and S. R. Helfrich (2004b), Estimating the distribution of snow water equivalent and snow extent beneath cloud-cover in the Salt-Verde River basin, Arizona, *Hydrol. Processes*, *18*, 1595–1611, doi:10.1002/hyp.1408.

Molotch, N. P., M. T. Colee, R. C. Bales, and J. Dozier (2005), Estimating the spatial distribution of snow water equivalent in an alpine basin using binary regression tree models: The impact of digital elevation data and independent variable selection, *Hydrol. Processes*, *19*, 1459–1479, doi:10.1002/hyp.5586.

Painter, T. H., J. Dozier, D. A. Roberts, R. E. Davis, and R. O. Green (2003), Retrieval of subpixel snow-covered area and grain size from imaging spectrometer data, *Remote Sens. Environ.*, *85*, 64–77.

Pinker, R. T., and I. Laszlo (1992), Modeling surface solar irradiance for satellite applications on a global scale, *J. Appl. Meteorol.*, *31*, 194–211.

Rango, A. (1988), Progress in developing an operational snowmelt-runoff forecast model with remote sensing input, *Nord. Hydrol.*, *19*, 65–76.

Rango, A., and J. Martinec (1982), Snow accumulation derived from modified depletion curves of snow coverage, in *Hydrological Aspects of Alpine and High Mountain Areas (Proceedings of the Exeter Symposium)*, *IAHS Publ.*, *138*, 83–89.

Rosenthal, W., and J. Dozier (1996), Automated mapping of montane snow cover at subpixel resolution from the Landsat thematic mapper, *Water Resour. Res.*, *32*, 115–130.

Shafer, B. A., C. F. Leaf, and J. K. Marron (1979), Landsat derived snow cover as an input variable for snow melt runoff forecasting in south central Colorado, in *Satellite Hydrology*, edited by M. Deutsch et al., pp. 218–224, Am. Water Resour. Assoc., Minneapolis, Minn.

Sicart, J. E., J. W. Pomeroy, R. E. Essery, J. Hardy, T. Link, and D. Marks (2004), A sensitivity study of daytime net radiation during snowmelt to forest canopy and atmospheric conditions, *J. Hydrometeorol.*, *5*, 774–784.

Thornton, P. E., S. W. Running, and M. A. White (1997), Generating surfaces of daily meteorological variables over large regions of complex terrain, *J. Hydrol.*, *190*, 214–251.

U.S. Army Corps of Engineers (1956), *Snow Hydrology: Summary Report of the Snow Investigations*, 462 pp., North Pac. Div., Portland, Oreg.

U.S. Soil Conservation Service (1972), Snow survey and water supply forecasting, in *Soil Conservation Service National Engineering Handbook*, pp. 1–7, U.S. Dep. of Agric., Washington, D. C.

Willmott, C. J., and K. Matsuura (1995), Smart interpolation of annually averaged air temperature in the United States, *J. Appl. Meteorol.*, *34*, 2577–2586.

Winstral, A., K. Elder, and R. Davis (2002), Spatial snow modeling of wind-redistributed snow using terrain-based parameters, *J. Hydrometeorol.*, *3*, 524–538.

R. C. Bales, Division of Engineering, University of California, Merced, CA 95344, USA. (bales@ucmerced.edu)

N. P. Molotch, Cooperative Institute for Research in Environmental Sciences, University of Colorado, Boulder, CO 80309, USA. (molotch@cires.colorado.edu)